

Joint Computational/Experimental Aerodynamic Study of a Simplified Tractor/Trailer Geometry

Subrahmanya P. Veluri, Christopher J. Roy, Aerospace and Ocean Engineering Department, Virginia Tech, 215 Randolph Hall, Blacksburg, Virginia, 24061, veluris@vt.edu (corresponding author)

Anwar Ahmed, Rifki Rifki, John C. Worley, and Bryan Recktenwald, Aerospace Engineering Department, Auburn University, 211 Aerospace Engineering Building, Auburn, Alabama, 36849-5338.

Abstract

Steady-state Reynolds Averaged Navier-Stokes (RANS) simulations are presented for the three-dimensional flow over a generic tractor trailer placed in the Auburn University 3ft- by 4 ft suction wind tunnel. The width of the truck geometry is 10 inches and the height and length of the trailer are 1.392 and 3.4 times the width, respectively. The computational model of the wind tunnel is validated by comparing the numerical results with the data from the empty wind tunnel experiments. The comparisons include the boundary layer properties at three different locations on the floor of the test section and the flow angularity at the beginning of the test section. Three grid levels are used for the simulation of the truck geometry placed in the test section of the wind tunnel. The coarse mesh consists of 3.4 million cells, the medium mesh consists of 11.2 million cells and the fine mesh consists of 25.8 million cells. The turbulence models used for both the empty tunnel simulations and the truck geometry placed in the wind tunnel are the standard Wilcox 1998 $k-\omega$ model, the SST $k-\omega$ model, the standard $k-\epsilon$ model and the Spalart-Allmaras model. The surface pressure distributions on the truck geometry and the overall drag are predicted from the simulations and compared with the experimental data. The computational predictions compared well with the experimental data. This study contributes a new validation data set and computations for high-Reynolds number bluff-body flows. The validation data set can be used for initial assessment in evaluating RANS models which will be used for studying the drag or drag trends predicted by the baseline truck geometries.

Introduction

The trucking industry is the backbone of the freight transportation system in the United States. According to 2003 data collected by the U.S. Department of Energy [1], there are approximately 2.2 million tractor-trailers operating on U.S. highways. These vehicles average 62,900 miles traveled per year at fuel consumption rate of 5.2 miles/gallon, resulting in an estimated consumption of 26 billion gallons of diesel fuel per year. With current diesel fuel costs near \$3.00/gallon, this translates into an annual cost of \$80 billion. In addition to the high costs

associated with transporting goods, the U.S. produces only 40% of the oil supplied to refineries. The remaining 60% is imported from other countries, with nearly half of all imports coming from the Organization of the Petroleum Exporting Countries (OPEC).

At typical highway speeds, roughly 60% of the truck engine's energy output goes to overcoming aerodynamic drag [2]. This is due to the fact that aerodynamic drag increases as the square of the vehicle speed, while the rolling resistance between the tires and the road increase linearly with the speed. Because it is such a large portion of the engine energy output at highway speeds, reductions in aerodynamic drag can significantly reduce the vehicle's fuel consumption. For example, a 25% reduction in the aerodynamic drag translates into a roughly 10% decrease in fuel consumed. When applied across the entire trucking industry, a 10% increase in fuel efficiency would save 2.6 billion gallons of diesel fuel per year, or approximately \$8 billion. To put these numbers in perspective, if we account for the fact that only approximately half of every barrel of crude oil is used to make diesel fuel, the U.S. imported the equivalent of 37 billion gallons of diesel fuel from OPEC in 2003 (nearly half of all U.S. imports). In addition to the economic impact and the implications on oil imports, increases in fuel efficiency also translate directly into reductions in pollution emissions and are thus more environmentally friendly.

There have been a number of studies which have examined the aerodynamic drag on tractor-trailers. In the 1970s and 1980s, the majority of this work was experimental in nature. A recent review of this work was presented by Cooper [3] who used both full-scale and sub-scale truck experiments to study the effects of various aerodynamic drag reduction devices for both the tractor and the trailer. More recently, researchers have also applied modern computational fluid dynamics (CFD) tools to study the aerodynamic drag of tractor-trailers. A recent DOE consortium has focused on both experimental methods and computational approaches to study the aerodynamic drag problem for trucks.[2] Their study resulted in high quality experimental data at near full-scale Reynolds numbers on two different geometries: the simplified Ground Transportation System (GTS) model [4] and the more realistic Generic Conventional Model (GCM) [5]. The simplified GTS model is an approximately 1/8 scale, class-8 tractor/trailer configuration which do not have any truck features on it with a smooth combined surface of the tractor and trailer (Figure 1). GCM is the representative of the class-8 tractor/trailer with the engine in front of the cab. The tractor geometry is the streamline-shaped representative of a modern tractor design without most of the small scale surface details. For this model, the tractor-trailer gap is present, but no under-carriage of the tractor or trailer are present which are replaced by a flat surfaces and also include the portion of the wheels below the tractor/trailer lower surface. The experiments were designed with the dual purpose of

evaluating drag reduction devices and also providing a high-quality experimental database for the validation of the CFD models. The primary modeling uncertainties are related to the choice for the turbulence model. The DOE consortium has examined the Reynolds-Averaged Navier-Stokes (RANS) approach, where all of the turbulent scales are modeled [6]-[8], and Large Eddy Simulation (LES), where the smaller turbulent scales are modeled but the larger scales resolved [9].

Much has been learned in the last 30 years of research on aerodynamic drag reduction for tractor-trailers. Reductions in aerodynamic drag are generally reported in terms of the drag coefficient

$$C_D = \frac{D}{\frac{1}{2}\rho_\infty V_\infty^2 S}$$

or possibly the wind-averaged drag coefficient, which accounts for variations in wind velocity and direction (see Ref. [3] for details). In the expression for the drag coefficient, D is the total drag on the truck, V_∞ is the free stream velocity, ρ_∞ is the free stream density and S is the frontal surface area of the truck. Drag reduction techniques such as cab side-extendors and cab roof air deflectors are commonly found on today's tractor-trailers and have resulted in wind-averaged drag coefficient reductions of up to 0.25 from the baseline value which is near unity. More advanced techniques such as tractor-trailer gap seals and trailer side skirts are less commonly seen on U.S. highways, but also can provide significant drag reduction. The remaining region where almost no drag reduction devices are found in use is the trailer base (immediately behind the trailer). This region is not aerodynamically efficient as compared to typical aerodynamic shapes (airfoils, tear drop shapes, etc.). Storms et al. [5] have shown experimentally that adding boat-tail plates or base flaps can further reduce the wind-averaged drag coefficient by 0.06; however, these add-on devices for the base region are not optimized configurations.

One way to optimize the drag reduction devices is to use CFD within some type of optimization strategy. This approach requires that the CFD tool be able to accurately predict the drag, or at least accurately predict the trends in the drag as the device is changed. The turbulence modeling approach that has the potential to produce the rapid turn-around time for drag reduction predictions is RANS, probably with wall functions used to alleviate the extremely fine wall spacing associated with integration of the turbulence modeling equations to the wall. The RANS turbulence modeling approach has been shown to accurately predict the drag for baseline configurations (i.e., without add-on base drag reduction devices); however, the details of the time averaged vortical structures and base pressure are very different from those found in experiment [6]. Because the details of the time-averaged flow are not correct, it is unclear whether RANS methods will accurately predict drag or even drag trends when drag reduction devices are included. More sophisticated turbulence modeling approaches such as

LES do appear to more accurately capture the details of the flow [10], but will be much too expensive to use as the primary aerodynamic prediction tool in a drag optimization strategy.

There are a number of open questions related to aerodynamic drag on tractor-trailers. For example, it is not clear what the theoretical minimum drag coefficient is for a tractor-trailer. Standard aerodynamics packages found on U.S. trucks have a wind-averaged drag coefficient of ~ 0.7 , while Ref. [3] indicates that additional proven technologies can further reduce this drag coefficient to ~ 0.55 . The most sophisticated modeling approach amenable to a design optimization process requiring a large number of solutions is the steady-state RANS approach. However, the ability of RANS methods to accurately predict drag and/or drag trends has not been proven. Furthermore, it is unclear if add-on drag reduction devices can be designed on simpler shapes than full-blown tractor-trailers. Finally, even if significant advances are made in aerodynamic drag reduction, how can we ensure that the resulting designs will be cost effective and see wide-spread use by the trucking industry?

Program Overview

Our research efforts on tractor-trailer aerodynamics are funded by the U.S. Department of Transportation and focus both on reducing fuel consumption (as discussed in detail above) and improving highway safety. Tractor-trailers can produce locally strong unsteady wind conditions that can be hazardous to smaller vehicles. The ultimate goal of this program is to use optimization methods to design add-on devices which reduce aerodynamic drag while at the same time reduce the large-scale fluctuation intensity in the vehicle wake. With increases in computing power, it is now becoming possible to use CFD as the aerodynamic prediction tool in a design optimization process. Part of our current research program is to demonstrate this CFD-based optimization capability [12]. The other aspect of current program is to examine the validity of RANS-based turbulence models for predicting drag (or drag trends) for tractor-trailers with add-on drag reduction devices. This aspect of the program includes both wind tunnel experiments and CFD analysis of simplified tractor-trailer geometry, and is the subject of the current paper. Various turbulence models run during the CFD analysis of the truck geometry in the wind tunnel are mentioned in Table 1.

Table 1. List of CFD simulations performed

CFD Simulations	Turbulence Models	Grids Used
Empty Wind Tunnel	k- ω	Coarse Grid (1,569,182 cells)
	SST k- ω	Fine Grid (4,643,435 cells)
Truck in Wind Tunnel	Spalart-Almaras	Coarse Grid (3,385,287 cells)
	k- ϵ	Medium Grid (11,179,943 cells)
	k- ω	Fine Grid (25,833,079 cells)
	SST k- ω	

Experimental Facilities

Tests were conducted in the Auburn University 3ft \times 4ft test section closed circuit wind tunnel capable of producing a maximum speed of 200 ft/s. Two types of wind tunnel truck models, each model consisted of a tractor and a trailer, were made from balsa wood reinforced with hardwood. The first model was finished with several layers of flat black paint for flow visualization purposes is shown in Figure 1. The same model was later used for the drag measurement. The second model was built for surface pressure distributions measurement. This model is equipped with 219 pressure taps, with 84 taps located on the tractor. 0.04 inch thick sandpaper was placed on the nose of the pressure model in order to obtain fully turbulent flow on the surface of the model. The schematic of the truck in the wind tunnel is shown in Figure 2.

Simplified Tractor/Trailer Geometry

The simplified tractor/trailer geometry was based on the Modified Ground Transportation System (MGTS) geometry developed by Hammache and Browand [11]. The simplified tractor/trailer geometry tested at Auburn University is a combination of a tractor with forward corners rounded to prevent flow separation and a rectangular trailer. The computational geometry of the simplified tractor/trailer placed in the wind tunnel test section is shown in Figure 3. The width of the trailer is 10 inches and the height to width ratio is 1.392. The length to width ratio of the trailer is 3.4, (this is a shorter trailer when compared to the actual trailers on road). A shorter trailer had to be used for the simulations due to the limitation of the test section length in the experiments. The target conditions are at Reynolds numbers greater than 1 million based on the trailer width since the drag and wake properties are independent of Reynolds number in this range [5]. There are six streamlined posts of height 4 in each on which the truck model stands. The height of the posts was chosen after conducting the empty tunnel

simulations and predicting the boundary layer height on the floor of the test section. It is desirable to know the boundary layer height on the floor of the test section to determine the position of the truck relative to the test section floor. In the case of truck on road, there will be no boundary layer developed on the road. In the computational simulations and the experiments, a moving ground plane is not employed. Considering the boundary layer developed on the floor of the test section and the bottom of the truck, a certain distance needs to be maintained between the truck bottom surface and the floor of the test section such that the boundary layers will not merge. The merging of the boundary layers leads to a fully developed flow under the truck and will affect the wake structure behind the truck.

Computational Fluid Dynamics Code

Mesh Generation

The Gridgen [15] grid generation tool is used for meshing the simplified tractor/trailer geometry and the empty wind tunnel. The wind tunnel surface geometry is found by taking measurements of the Auburn University wind tunnel and the surface definition is imported into Gridgen. Two different meshes levels are considered for the empty wind tunnel. The coarse mesh has approximately 1.5 million cells and the fine mesh has approximately 4.6 million cells. Initially a structured quadrilateral mesh is used on the surface of the wind tunnel. Before generating the volume mesh, the height of the first layer of cells from the wind tunnel surface is determined such that the y^+ values are close to 1 for both the meshes. Empty wind tunnel simulations are run to compare computed flow angularity and boundary layer properties with the experimental data.

In the simulations which involved the truck geometry in the wind tunnel, three mesh levels termed as coarse, medium and fine are used. The coarse, medium and fine meshes consist of approximately 3.4 million, 11.2 million and 25.8 million cells, respectively. Most of the meshing is done using a structured mesh except for some regions in the front of the truck (well outside the boundary layer) which are meshed using an unstructured grid. The reason for mostly using structured grid is that, it is easy to uniformly refine/coarsen the mesh which is required for solution verification purposes [21]. Comparatively, it is difficult to uniformly refine an unstructured mesh with tetrahedral cells and it cannot be achieved when meshing is done using commercial software. Also it is advisable to use structured hexahedral cells in the boundary layer flow as structured meshes do a better job in resolving the boundary layer flow when compared to the unstructured meshes.

Discretization

The steady-state RANS simulations are conducted on the empty wind tunnel geometry using the Fluent [16] CFD code. A segregated solver is used for the computations which employs a cell-centered finite volume method. A second-order accurate upwind discretization is used for the momentum equation, turbulent kinetic energy equation and specific dissipation rate equation [16] for all the simulations except for the standard k- ϵ model on the fine mesh, where, only a first-order accurate upwind discretization is used for the turbulent kinetic energy equation and turbulent dissipation rate equations, since convergence is not achieved with the second-order upwind discretization. The SIMPLE algorithm [16] is used to obtain a relationship between velocity and pressure corrections to enforce mass conservation and to obtain the pressure field.

Boundary Conditions

In the case of the empty wind tunnel, the velocities are close to Mach 0.1 and as there is not much variation in the temperature, the flow is considered incompressible during the simulations. At the inlet, a stagnation pressure boundary condition is applied. A gauge pressure value of 0.248846 psi (1715.733 N/m²) measured from the experiments is used. The outlet boundary condition is set to atmospheric. The tunnel walls are defined as stationary no-slip walls with a surface roughness of 0.015748 inch (0.4 mm) to achieve a better agreement with the actual rough wall in the experiments. The boundary conditions during the simulations are applied such that the conditions match the empty wind tunnel experiments conducted at Auburn University.

The turbulence models used are the standard Wilcox 1998 k- ω model [18], the SST k- ω model, the standard k- ϵ model and the Spalart-Allmaras model. The free stream turbulence parameters, k , ω and ϵ are calculated using the formulae from Ref. 17. To determine these parameters, a turbulent intensity (T_u) of 1% and the ratio of turbulent to laminar viscosity equal to 10 are considered. The turbulent intensity used in the computations is measured for the wind tunnel. The values of k , ω and ϵ calculated are 0.18816, 1288.119, and 17.801, respectively. The formulae for calculating the turbulent kinetic energy, k and the specific dissipation rate, ω are

$$k = \frac{1.2}{2} \left(\frac{T_u}{100} \right)^2 V_\infty^2 \quad \omega = \frac{\left(\frac{\rho k}{\mu} \right)}{\left(\frac{\mu_t}{\mu} \right)}$$

In the expression for the calculation of specific dissipation rate, ρ is the density, k is the turbulent kinetic energy, μ_t is the turbulent viscosity and μ is the laminar viscosity

Results

Results include both the computational predictions and the experimental data of the flow properties in the empty wind tunnel and also with the truck model placed in the wind tunnel test section. The empty wind tunnel results consist of the measurements of flow angularity at the beginning of the test section and the boundary layer properties on the floor of the test section. The truck simulations include the surface pressure distribution on the truck geometry and the overall drag prediction and are compared with the experimental data.

Empty Wind Tunnel Simulations

The empty wind tunnel simulations are done to validate the computational model of the wind tunnel by comparing the computational predictions with the data from the empty tunnel experiments. Another purpose of conducting the empty tunnel simulations is to find the boundary layer height on the floor of the test section to determine the position of the truck relative to the test section floor. The Auburn University wind tunnel consists of a 3ft × 4ft test section which has a length of 65 in. The upstream portion of the test section gradually changes from a circular cross-section to a rectangular cross-section as the flow enters the test section. Immediately downstream of the test section is a small gap which is opened to the atmosphere. The turning vanes which are used for diverting the flow in the axial direction upstream of the contracting section are not considered in the computations, but are replaced by a flat surface which is at a 45° angle with the axial flow direction. A top view of the wind tunnel showing the vanes which turn the flow is shown in Figure 4.

Computational Predictions

The steady-state RANS simulations are conducted on the empty wind tunnel geometry using Fluent [18]. The empty tunnel simulations are performed to validate the computational model of the wind tunnel. Empty wind tunnel simulations are carried out to find the boundary layer height from the test section floor. The boundary layer properties are predicted at three different locations on the floor of the test section. The boundary layer heights at 9, 20 and 39 in from the beginning of the test section are predicted to be 0.772, 0.975 and 1.33 in, respectively. In the simulations, a surface roughness of 0.015748 inch (0.4 mm) is used to achieve a better agreement with the boundary layer properties from the experiments. After the comparisons it was decided to place the truck geometry at a height of 4 inches from the test section floor. Hence, the stream-lined posts on which the truck geometry stands were set to a height of 4 inches. This height of the posts is also matched in the computations.

The empty tunnel simulations are converged until the iterative error in the simulations is considered small. The convergence criterion for the continuity equation is 5×10^{-6} and it is set to 1×10^{-6} for the momentum, k and ω equations. These convergence criteria are found by monitoring the estimated numerical error in the drag. When the error in the drag becomes lower than 0.01%, then the required convergence levels are set.

Model Validation

The numerical predictions are compared with the experimental results for the validation of the model. The validation of the computational model of the empty wind tunnel includes the comparison of the boundary layer properties at the three locations on the floor of the test section and the flow angularity at the beginning of the test section with the experimental data. The boundary layer thickness, the displacement thickness, and momentum thickness at 9, 20 and 39 in from the beginning of the test section on the wind tunnel floor are compared with the experimental results. The boundary layer properties predicted from the computations are compared with the experimental data and are tabulated in Table 2. The boundary layer properties matched closely with the experimental data except for the boundary layer height at the farthest downstream section. A higher value of boundary layer thickness is observed in the experiments at the last station, i.e. 39 in from the beginning of the test section, possibly due to the highly rough surface present on the test section floor at that location. The boundary layer profiles from the computations are compared with the experimental measurements at the three locations and are shown in Figure 5.

Table 2. Comparison of numerical results of boundary layer properties with experimental results

Boundary layer properties (inches)		Numerical	Experimental	Percentage Error
Beginning of the test section X = 9 in	δ_{99}	0.772	0.76	-1.58
	δ^*	0.1426	0.13	-9.69
	Θ	0.0985	0.11	10.45
End of the tractor X = 20 in	δ_{99}	0.975	0.96	-1.56
	δ^*	0.1794	0.18	0.33
	Θ	0.126	0.15	16
End of the trailer X = 39 in	δ_{99}	1.33	1.56	14.74
	δ^*	0.2313	0.23	-0.56
	Θ	0.1651	0.20	17.45

The flow angularity data in the experiments at the beginning of the test section are matched with the flow angularity prediction from the computations by changing the flow angle at the inlet boundary condition in the computations and it is observed that an inlet flow angle of 20 degrees with the axial direction shows better agreement when compared with the other flow angles. Different flow angles at the inlet had to be tested to match the flow angularity at the beginning of the test section, since there is no information on the flow direction and behavior of the flow at the vanes in the experiments. The flow angularity comparison at 9 in from the beginning of the test section at the vertical centerline location is shown in Figure 6.

Truck Simulations

Computational Predictions

For the RANS simulations of the truck geometry in the wind tunnel, an extended test section is considered in order to move the outflow boundaries sufficiently far away from the truck wake. The test section length is made twice the actual length in the experiments. The simulations are carried on three mesh levels. The coarse, medium and fine meshes consists of approximately 3.4 million cells, 11.2 million cells and 25.8 million cells, respectively. The computational mesh (coarse grid) with the truck geometry placed in the wind tunnel test section is shown in Figure 7.

The simulations are conducted at a Reynolds number approximately equal to 1 million based on the trailer width in order to match the value used in the experiment. The drag has been found to be independent of Reynolds number above this range [5]. All four turbulence models are tested on both the coarse and medium grids: the standard Wilcox 1998 $k-\omega$ model [16], the SST $k-\omega$ model [16], the standard $k-\epsilon$ model [16] and the Spalart-Allmaras [16]. Only two turbulence models, the SST $k-\omega$ model [16] and the standard $k-\epsilon$ model [16], are tested on the fine mesh. The stagnation pressure and temperature values are set at the 45° inlet plane to match the stagnation conditions in the wind tunnel and the back pressure is varied at the outlet to match the reference pressures. The truck walls and the tunnel walls are defined as no slip walls with a surface roughness of 0.015748 inch (0.4 mm) on the tunnel walls. With these boundary conditions, a static pressure very close to atmospheric is achieved at the cross section downstream of the test section where there is a gap in the actual wind tunnel. Also, the back pressure is varied such that the pressure values at three locations in the upstream region of the test section are matched, which are initially considered as the reference pressures. Later, the pressure values are replaced by the pressure value on the top of the trailer surface as the reference pressure and the reference pressure on the trailer surface is used for the calculation of the pressure coefficient and the drag coefficient. This change

has to be made because the three reference pressure locations in the upstream region of the test section are too close to the truck geometry, and are located at the beginning of the test section after the converging portion of the wind tunnel. Their use requires a highly accurate simulation of the pressure variations at that location because of the acceleration of the flow due to presence of the truck geometry.

Before comparing the results from the computations with the experiments, it is important to estimate the numerical errors. The turbulence cases are initially converged using a first-order spatial discretization, and then subsequently restarted with a second-order discretization. It is observed from the residuals that the convergence is rather slow when the second-order upwind discretization [16] is used as compared with the first-order discretization. The convergence of the residuals is faster for the first-order scheme due to additional dissipation, but for the second order scheme, the residuals do not converge to steady state due to the unsteady wake that was found to form behind the posts and the truck.

To find out whether the solution is converged, the drag variation with iterations is examined and it can be seen that the drag values oscillate along a constant mean value. The behavior of drag on the truck with the iterations is shown in Figure 8. The source of oscillations is the unsteady flow behind the truck base and the posts. Even behind the posts, there is a flat rear surface which leads to separation and hence the oscillations in the drag convergence. When the drag is no longer converging, and only oscillating about a constant mean value, the pressure coefficient and the drag coefficient are calculated. The pressure values on the top, bottom, sides, front and backside of the truck are extracted to calculate the pressure coefficient. The pressure coefficient is calculated using the formula:

$$C_p = \frac{p - p_{ref}}{\frac{1}{2} \rho_{\infty} V_{\infty}^2}$$

where, p is the static pressure, p_{ref} is the reference pressure.

The overall drag-coefficient calculated using all four turbulence models for the different mesh levels is tabulated in Table 3. To get an error estimate on the numerical solution, Grid Convergence Index (GCI) values are calculated for the medium and fine mesh solutions and the calculated values are tabulated in Table 3. A GCI value on a fine grid solution, proposed by Roache [20], is defined as:

$$GCI = \frac{F_s}{r^p - 1} \left| \frac{f_2 - f_1}{f_1} \right|$$

where F_s is the factor of safety, f_1 and f_2 are the finer grid solution and the coarser grid solutions, respectively, r is the refinement factor between the two grids considered and p is the observed order of accuracy. The refine-

ment factor is 1.5 between the coarse and medium meshes and it is 1.33 between the medium and fine meshes. The observed order of accuracy cannot be calculated using 2 grids and hence in the case of the standard Wilcox 1998 k- ω and the Spalart-Allmaras turbulence models, the observed order of accuracy is assumed to be equal to formal order of two. For this case, Roache [13] recommends a conservative factor of safety value of $F_s = 3$. For the SST k- ω and the standard k- ϵ turbulence models, there are solutions from three grid levels and hence an observed order of accuracy value can be calculated. In this case, the GCI can be calculated using the calculated observed order of accuracy. Assuming the observed order of accuracy matches the formal order, a less conservative factor of safety of 1.25 can be used for these cases. The GCI converts the estimate of the error in the numerical solution into an error of uncertainty band. The observed order of accuracy is 2.32 for the SST k- ω turbulence model and 1.166 for the k- ϵ turbulence model. In the case of k- ϵ turbulence model, the k- and ϵ -equations are run first order as the residuals diverged when they are run second order upwind scheme. The reduction in the order of accuracy may be due to first order convergence of the k- and ϵ -equations. The formula used for the calculation of order of accuracy is given below:

$$\frac{f_3 - f_2}{r_{23}^p - 1} = r_{12}^p \left(\frac{f_2 - f_1}{r_{12}^p - 1} \right)$$

where f_1 is the fine grid solution, f_2 is the medium grid solution, f_3 is the coarse grid solution, r_{12} is the refinement factor between the fine and medium grids and r_{23} is the refinement factor between the medium and coarse grids. Observed order of accuracy, p in the equation is obtained using a Newton-Raphson method.

Table 3. Computational prediction of the overall drag coefficient using different turbulence models

	Drag Coefficient, C_D			GCI
	Coarse Mesh	Medium mesh	Fine Mesh	
Spalart-Almaras	0.4039	0.3975	-	6.28%
k- ϵ	0.3124	0.3088	0.3072	1.14%
k- ω	0.3139	0.3089	-	13.14%
SST k- ω	0.3088	0.3024	0.3003	0.56%

Experimental Results

Due to limited data acquisition resources, the surface pressure measurements were done in two stages. The first stage measured the surface pressure distribution on the tractor through the 84 pressure taps located on the

tractor, and the second measured the surface pressure distribution on the trailer. In both stages, pressure taps were connected to Scanivalve Corp. 48 port pressure scanners by plastic pressure tubes. All tubes were made to have an equal length, approximately 4ft, in order to minimize differences in pressure reading due to the resonance effect. The pressure scanners were connected to a Scanivalve Corp. DSA-3217 that has 16 pressure transducers. Only five to six transducers were used for tractor or trailer pressure measurements respectively, with three transducers dedicated to measure the reference pressures discussed earlier. The sampling frequency of the DSA-3217 was 0.5 Hz/channel. The maximum uncertainty of the pressure measurement was calculated to be 5%.

Force measurements were conducted using an external pyramidal force balance. Calibration of the balance was performed and verified within an accuracy of 2.0%. The model was attached to an adapter plate which was connected securely to the top of the pyramidal balance. The struts were connected firmly to the wind tunnel floor leaving a gap of a 1/16 inch between the strut and model. This allowed for free movement of the model and balance during dynamic forces. A Lab view program was written to run these tests while data was collected through a D/A board.

Collecting the data from the experiments, the overall drag coefficient is calculated. The experiment is repeated several times to test the repeatability. The average drag measured from the experiments is 12.53 lbf. The atmospheric pressure and density measured during the experiments are 14.2866 psi and 0.002198 slug/ft³, respectively. The average value of the overall drag coefficient calculated from the experimental data is 0.325. The experimental uncertainty is estimated to be 5% and hence with the error bounds the average drag coefficient from the experiments is reported as 0.325 ± 0.016 .

Model Validation

The pressure distribution on the truck model from the simulations is compared with the experimental measurements from the ports located at various positions on the truck geometry. The location of the pressure taps on the truck geometry is shown schematically in Figure 9. The pressure distributions include the C_p variations on the top, bottom, sides, front and back of the truck geometry. The comparison of C_p of the two turbulence models (SST $k-\omega$ and standard $k-\epsilon$) for the fine mesh to the experimental measurements on the top and bottom of the truck geometry is shown in Figure 10. Similarly, the comparison of the C_p values of the two turbulence models to the experimental measurements on the two sides of the truck geometry is shown in Figure 11. The C_p comparisons on the front side and back side are shown in Figure 12 and Figure 13, respectively. The deviation of the experimental data of the C_p values from the computations on the front of the truck is due to the difficulty in the

measurement of the port location on the curvature. On the back of the trailer, the turbulence models did not accurately predict the behavior of the flow when compared to the experiments and hence the difference in the C_p comparisons. The turbulence models predicted a symmetric pair of counter-rotating vortices on the back of the trailer, but from the pressure distribution in the experiments, it looked like the counter-rotating vortices have a different structure which is not symmetric and only one large vortex seems to be present exactly behind the trailer. The velocity contours along with the streamlines on the vertical symmetry plane at the back of the trailer for the SST $k-\omega$ turbulence model are shown in Figure 14. The pressure contours on the back side of the trailer compared with the pressure data at the port location from the experiments are shown in Figure 15. The contours in the circular spots show the pressure values from the experimental data at the port locations. The comparison shows a higher negative pressure towards the top and bottom of the trailer back surface in the computations, but a higher negative pressure only towards the bottom of the trailer back surface which represent an asymmetric flow behavior in the experiments behind the trailer.

Initially, the reference pressures at three different locations in the test section, one on the floor, and the other two on the side walls of the test section are obtained from the simulations and compared with the experimental data. Later the location of the reference pressure is changed to one of the ports on the top of the trailer. The reason for this change in the location of the reference pressure is that the three ports initially considered on the wind tunnel test section fall in the region of high pressure variations. They are located on the test section at the beginning of the truck where the flow is accelerated due to the presence of the truck geometry. Hence the reference pressure position is changed to the location on the top of the trailer.

Finally the drag coefficient predicted from the simulations, for Wilcox 1998 $k-\omega$ and the Spalart-Allmaras turbulence models on the medium mesh and the SST $k-\omega$ model and the standard $k-\epsilon$ model on the fine mesh, is compared with the experimental result. The comparison of the drag coefficient along with the percentage error in their mean predictions relative to the experiment is shown in Table 4.

Table 4. Drag coefficient comparison

	Drag Coefficient, C_D	% Error
Spalart-Almaras	0.3975 ± 0.0249	- 22.3 %
$k-\epsilon$	0.3072 ± 0.0035	5.48 %
$k-\omega$	0.3089 ± 0.0405	4.95 %
SST $k-\omega$	0.3003 ± 0.0017	7.6 %
Experiments	0.325 ± 0.016	-

Conclusions

RANS simulations were performed on the empty wind tunnel geometry and the truck model placed in the wind tunnel. The boundary layer height in the wind tunnel test section was calculated to determine the position of the truck geometry relative to the test section floor. The boundary layer properties on the floor along the test section length and the flow angularity at the beginning of the test section were predicted and compared with the experiments carried out in the 3-ft by 4-ft Auburn University wind tunnel for validation. After the calculation of the boundary layer height from the test section floor, the tractor/trailer geometry was placed at a height of 4 inches from the test section floor.

The steady-state Reynolds Averaged Navier-Stokes (RANS) simulations over the Modified Ground Transportation System placed in the 3-ft by 4-ft Auburn University wind tunnel were conducted to predict the surface pressure distribution on the truck geometry and the overall drag. The computational predictions are compared with the experimental data for validation. The surface pressure distributions from the computations agreed reasonably well with the experimental data except in the base region. The RANS models predicted a symmetric pair of counter rotating vortices behind the trailer but from the pressure distribution in the experiments, it looked like there is only one large vortex in the trailer base region. The behavior in the computations is consistent with other RANS simulations of high Reynolds number bluff-body flows [6], [7], [9]. Also, the overall drag is predicted well by the RANS two equation models: the standard Wilcox 1998 $k-\omega$ model, the SST $k-\omega$ model and the standard $k-\epsilon$ model. The Spalart-Allmaras model over-predicted the overall drag value and the drag coefficient value is 22.3% higher than the experimental value.

Acknowledgements

We would like to thank Andy Weldon of Auburn University for his invaluable help in building the truck model and his aid with the experimental set up. This work was supported by the U.S. Department of Transportation's Federal Motor Carrier Safety Administration (FMCSA) under Grant No.MH-05-01-1 with Mr. Chris Flanigan serving as the technical monitor.

References

- [1] US DOE Transportation Energy Data Book: Edition z23, 2003, <http://www-cta.ornl.gov/data/>
- [2] R. C. McCallen, K. Salari, J. M. Ortega, L. J. DeChant, B. Hassan, C. J. Roy, W. D. Pointer, F. Browand, M. Hammache, T.-Y. Hsu, A. Leonard, M. Rubel, P. Chatalain, R. Englar, J. Ross, D. Satran, J. T. Heineck, S. Walker, D. Yaste, and B. Storms, "DOE's Effort to Reduce Truck Aerodynamic Drag – Joint Experiments and Computations Lead to Smart Design," AIAA Paper 2004-2249, 34th AIAA Fluid Dynamics Meeting, Portland, OR, June 2004.
- [3] Cooper, K. R., 2003, "Truck Aerodynamics Reborn – Lessons from the Past," SAE Paper 2003-01-3376.
- [4] Storms, B. L., Ross, J. C., Heineck, J. T., Walker, S. M., Driver, D. M., and Zilliac, G. G., 2001, "An Experimental Study of the Ground Transportation System (GTS) Model in the NASA Ames 7- by 10-ft Wind Tunnel," NASA TM-2001-209621.
- [5] B. Storms, D. Satran, J. Heineck and S. Walker, "A Study of Reynolds Number Effects and Drag-Reduction Concepts on a Generic Tractor-Trailer," AIAA-2004-2251, June 28-1, 2004.
- [6] C. J. Roy, J. L. Payne, and M. A. McWherter-Payne, "RANS Simulations of a Simplified Tractor-Trailer Geometry," *ASME Journal of Fluids Engineering*, Vol. 128, 2006, pp.1083-1089.
- [7] Salari, K., Ortega, J. M., and Castellucci, P. J., 2004, "Computational Prediction of Aerodynamic Forces for a Simplified Integrated Tractor-Trailer Geometry," AIAA Paper 2004-2253.
- [8] W. Pointer, "Evaluation of Commercial CFD Code Capabilities for Prediction of Heavy Vehicle Drag Coefficients," AIAA-2004-2254, June 28-1, 2004.
- [9] C. J. Roy, J. C. Brown, L. J. DeChant, and M. A. Barone, "Unsteady Turbulent Flow Simulations of the Base of a Generic Tractor-Trailer," AIAA Paper 2004-2255, June 2004.
- [10] Unaune, S. V., Sovani, S. D., and Kim, S. E., "Aerodynamics of a Generic Ground Transportation System: Detached Eddy Simulation," SAE Paper 2005-01-0548.
- [11] Hammache, M., Browand, F., "On the Aerodynamics of Tractor-Trailers," *The Aerodynamics of Heavy Vehicles: Trucks, Buses and Trains*, edited by R. C. McCallen, F. Browand, and J. C. Ross, Lecture Notes in Applied and Computational Mechanics, Vol. 19, Springer-Verlag, Heidelberg, 2004.
- [12] Doyle, J. B., Hartfield, R. J., and Roy, C. J., "Tractor Trailer Optimization by a Genetic Algorithm with CFD," AIAA Paper 2006-3863, June 5-8, 2006.
- [13] Roache, P. J., *Verification and Validation in Computational Science and Engineering*, Hermosa Publishers, New Mexico, 1998.
- [14] Roy, C. J., "Review of Code and Solution Verification Procedures in Computational Simulation," *Journal of Computational Physics*, Vol. 205, No. 1, 2005, pp. 131-156.
- [15] Gridgen User Manual, Version 15, Pointwise Inc., Forth Worth, TX.
- [16] Fluent 6.1 User's Guide, Fluent Inc., Lebanon, NH, 2003.
- [17] C. J. Roy and F. G. Blottner, "Methodology for Turbulence Model Validation: Application to Hypersonic Flows", *Journal of Spacecraft and Rockets*, Vol. 40, No.3, 2003, pp.313-325.
- [18] D. C. Wilcox, *Turbulence Modeling for CFD*, 2nd Edition, DCW Industries, Inc., La Canada, California, 1998.
- [19] Veluri, S. P., Roy, C. J., Ahmed, A., and Rifki, R., "Preliminary RANS Simulations and Experimental Study of a Tractor-Trailer Geometry," AIAA Paper 2006-3857, San Francisco, CA, June 2006.
- [20] Roache, P. J., "Perspective: A Method for Uniform Reporting of Grid Refinement Studies," *Journal of Fluids Engineering*, Vol. 116, 1994, pp. 405-413.
- [21] Salas, M. D., "Some observations on grid convergence," *Computers and Fluids*, Vol. 35, 2006, pp. 688-692.

Figures



Figure 1: Flow visualization/force model mounted in the wind tunnel test section

Subrahmanya Veluri
Joint Computational/Experimental Aerodynamic Study of a Simplified Tractor/Trailer Geometry

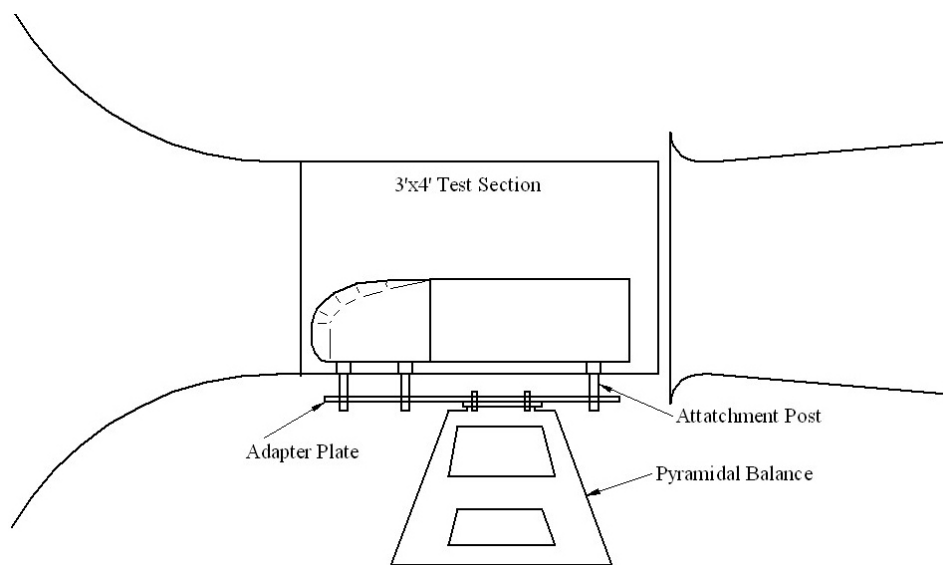


Figure 2: Schematic of the simplified truck geometry in the wind tunnel

Subrahmanya Veluri
Joint Computational/Experimental Aerodynamic Study of a Simplified Tractor/Trailer Geometry

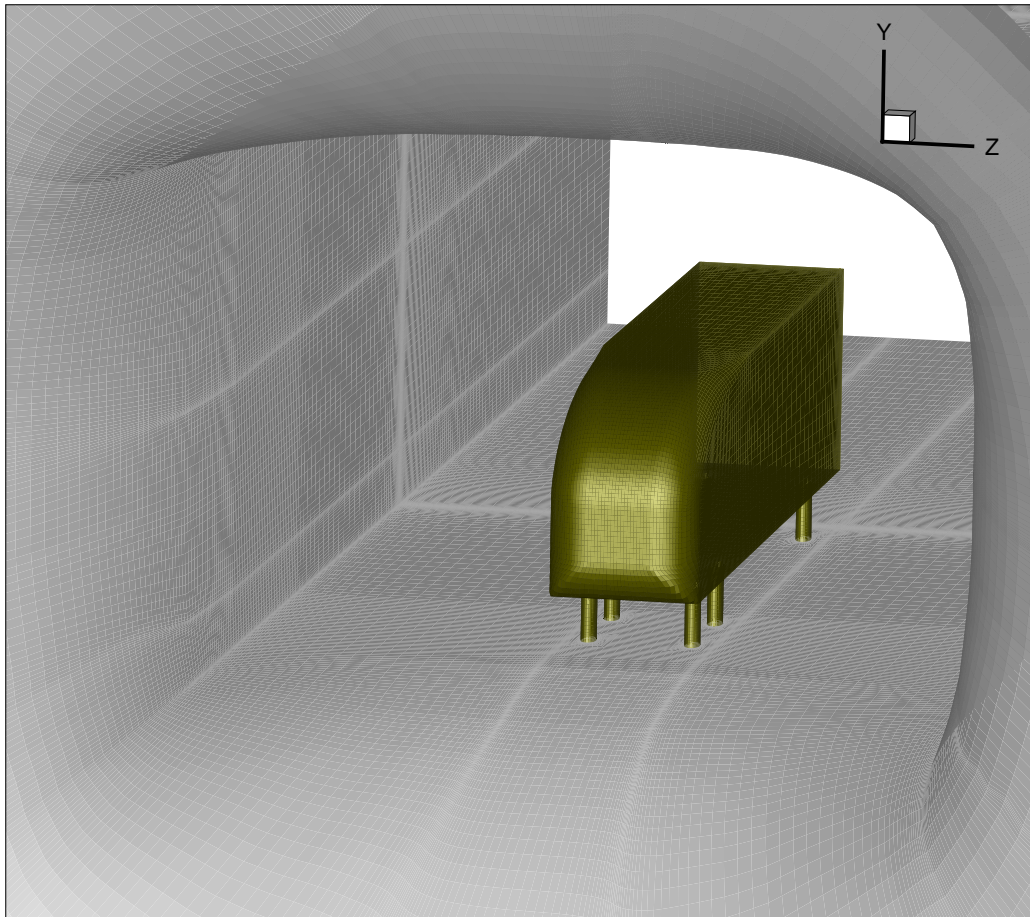


Figure 3: Computational geometry of the simplified tractor/trailer placed in the wind tunnel

Subrahmanya Veluri

Joint Computational/Experimental Aerodynamic Study of a Simplified Tractor/Trailer Geometry

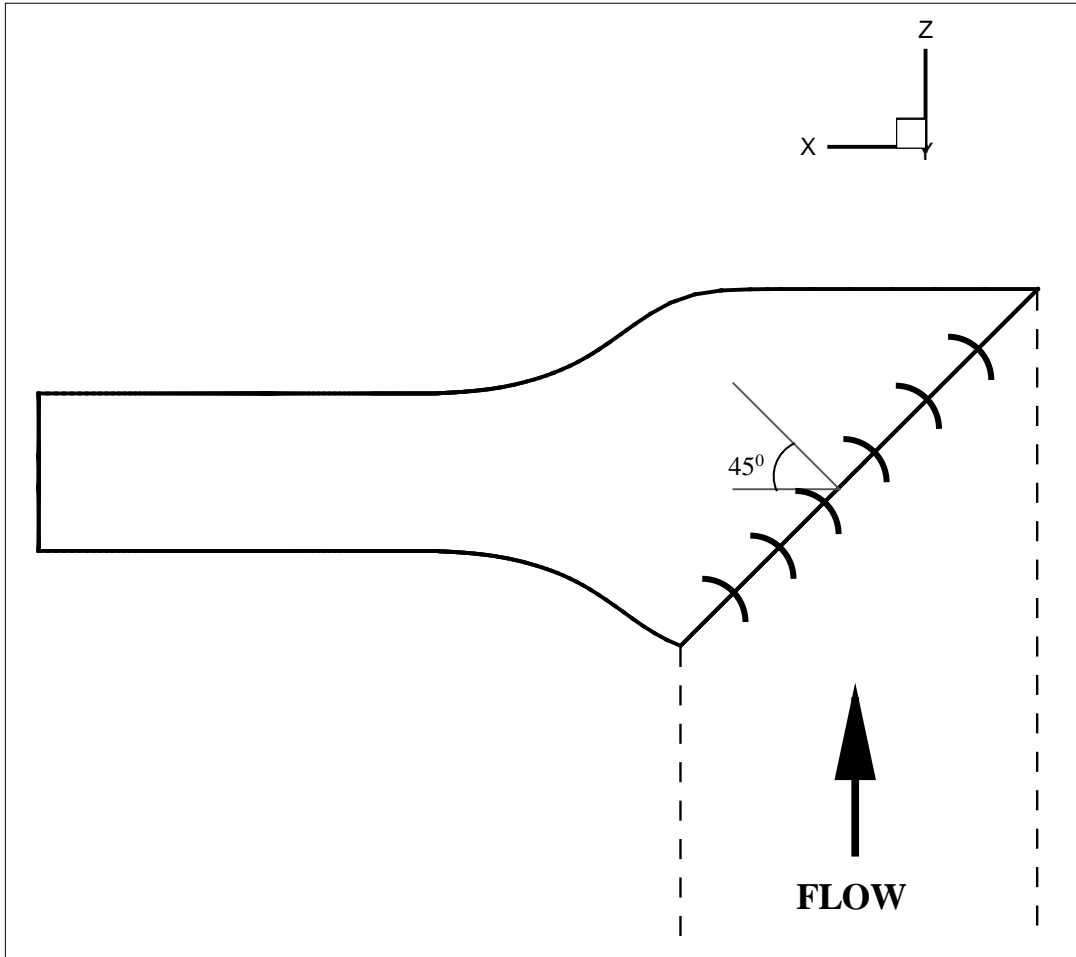


Figure 4: Top view of the wind tunnel geometry

Subrahmanya Veluri
Joint Computational/Experimental Aerodynamic Study of a Simplified Tractor/Trailer Geometry

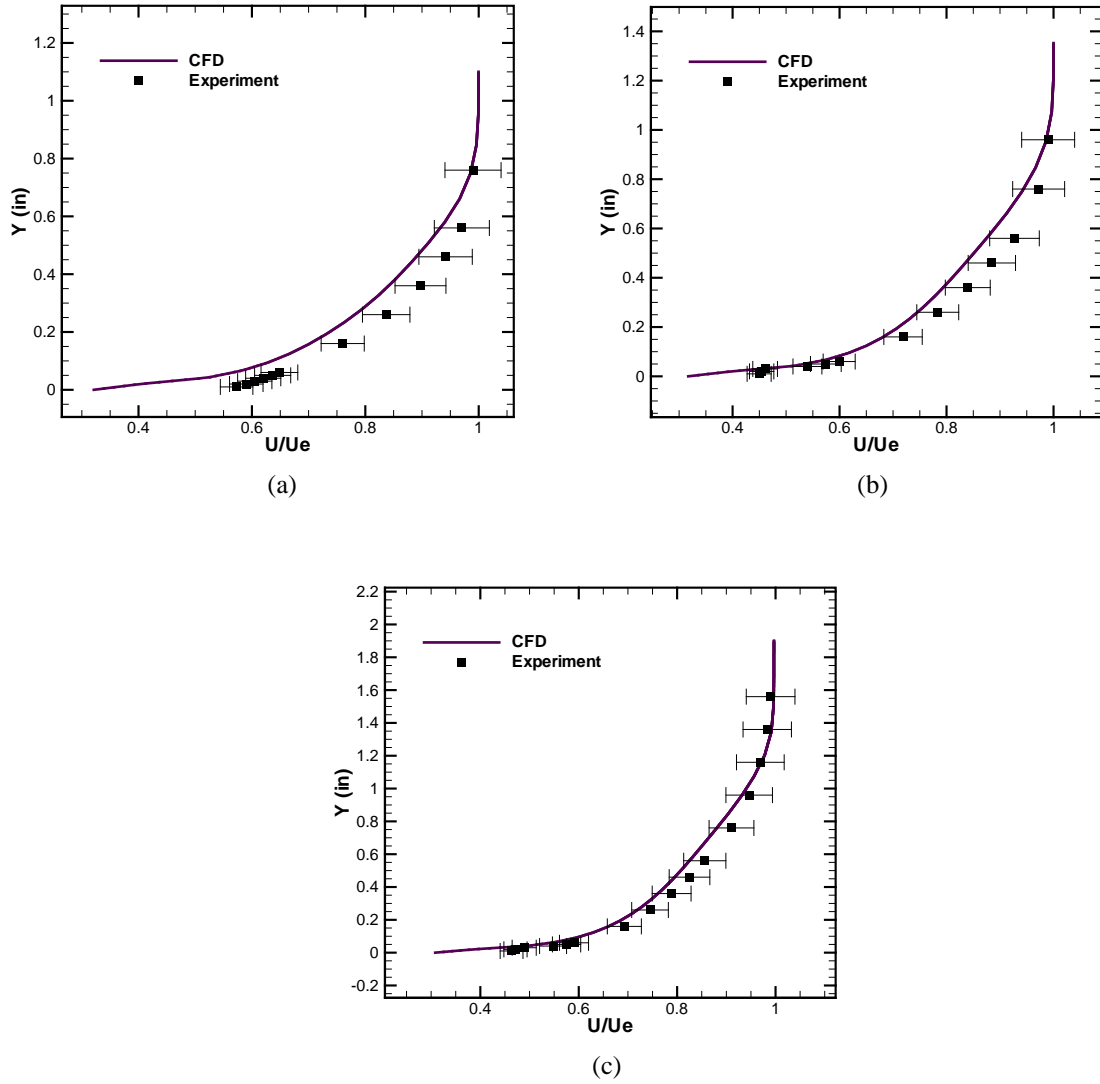


Figure 5: Comparison of boundary layer profiles (a) at 9 in (b) at 20 in (c) at 39 in from the beginning of the test section

Subrahmanya Veluri
 Joint Computational/Experimental Aerodynamic Study of a Simplified Tractor/Trailer Geometry

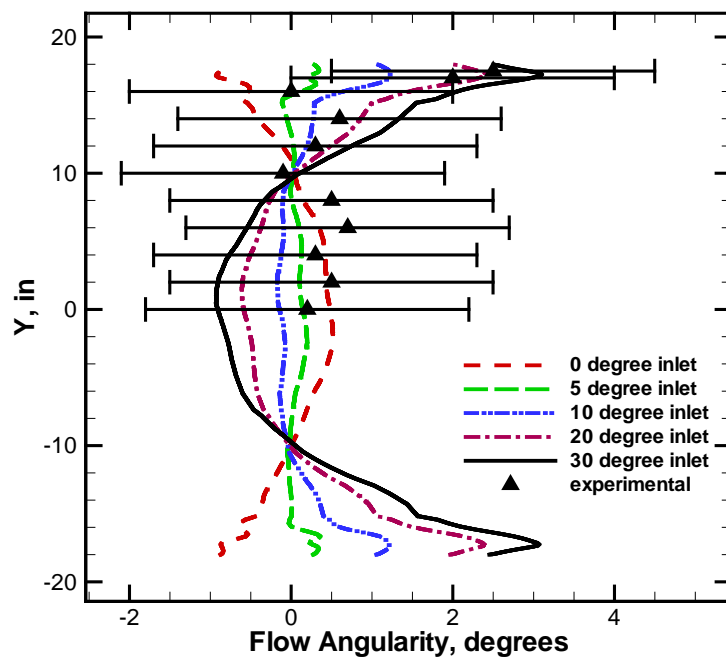


Figure 6: Flow angularity at vertical center at 9 inches from the beginning of the test section

Subrahmanya Veluri

Joint Computational/Experimental Aerodynamic Study of a Simplified Tractor/Trailer Geometry

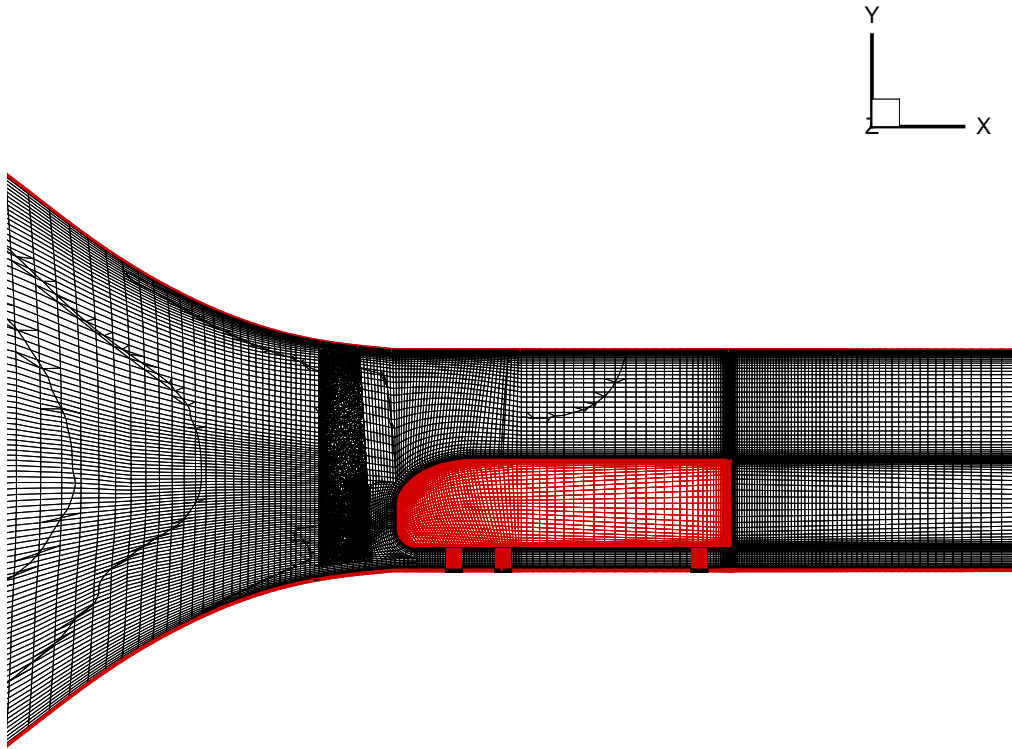


Figure 7: Computational mesh (coarse grid) for the truck geometry placed in the wind tunnel

Subrahmanya Veluri

Joint Computational/Experimental Aerodynamic Study of a Simplified Tractor/Trailer Geometry

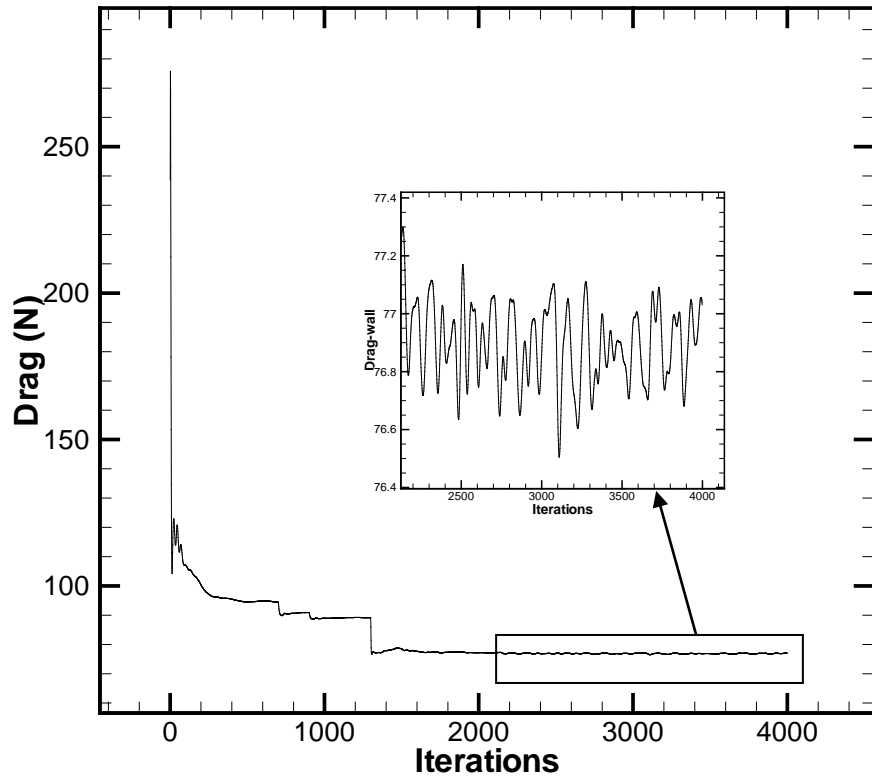


Figure 8: Drag convergence on truck

Subrahmanya Veluri
Joint Computational/Experimental Aerodynamic Study of a Simplified Tractor/Trailer Geometry

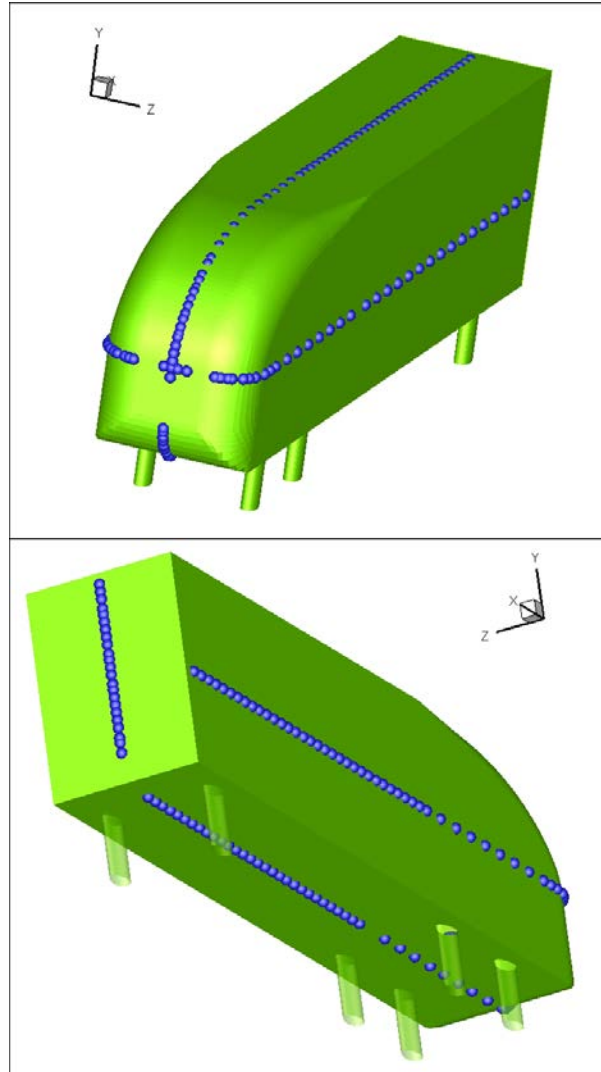


Figure 9: Schematic of the location of the pressure ports on the truck geometry

Subrahmanya Veluri

Joint Computational/Experimental Aerodynamic Study of a Simplified Tractor/Trailer Geometry

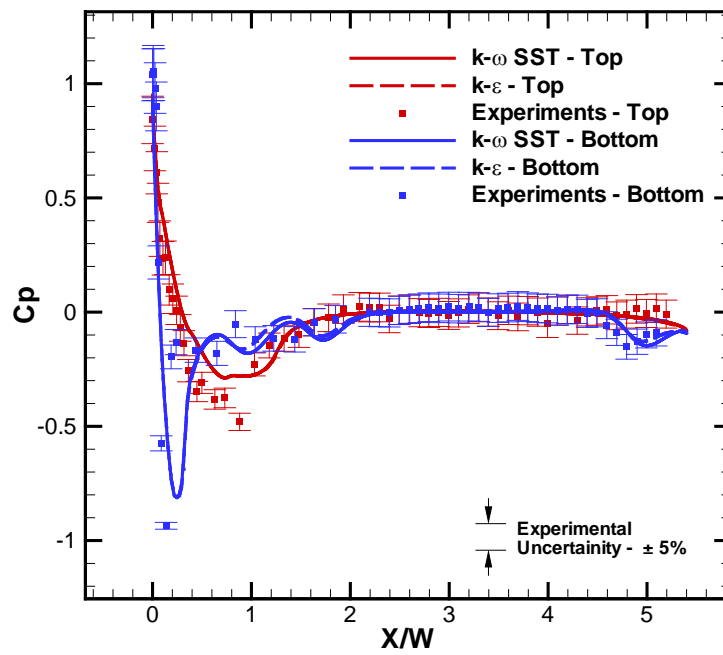


Figure 10: Comparison of the C_p variation on the top and bottom of the truck geometry

Subrahmanya Veluri
 Joint Computational/Experimental Aerodynamic Study of a Simplified Tractor/Trailer Geometry

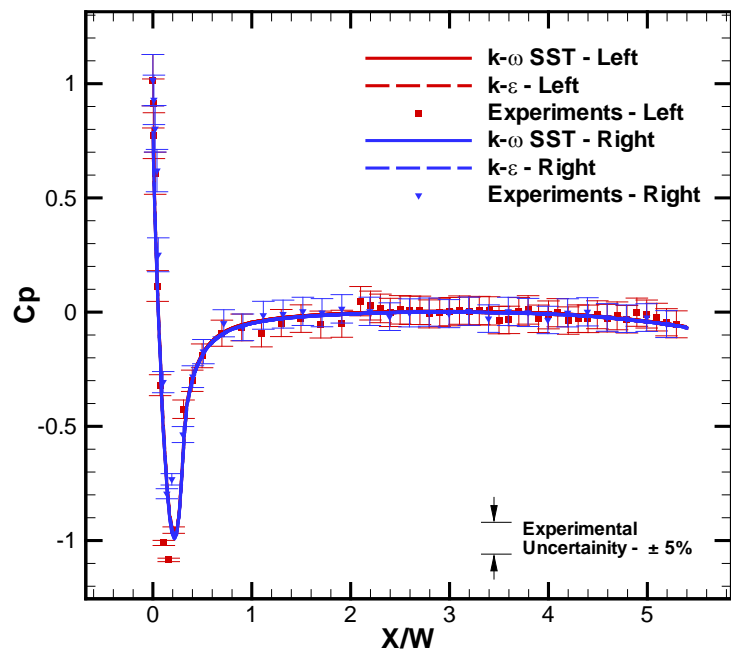


Figure 11: Comparison of the C_p variation on the sides of the truck geometry

Subrahmanya Veluri

Joint Computational/Experimental Aerodynamic Study of a Simplified Tractor/Trailer Geometry

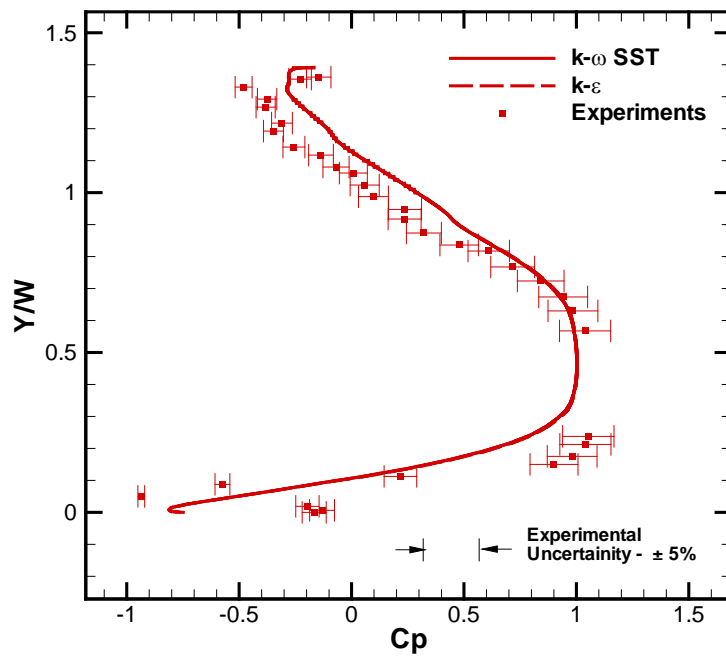


Figure 12: Comparison of the Cp variation on front of the truck geometry

Subrahmanya Veluri

Joint Computational/Experimental Aerodynamic Study of a Simplified Tractor/Trailer Geometry

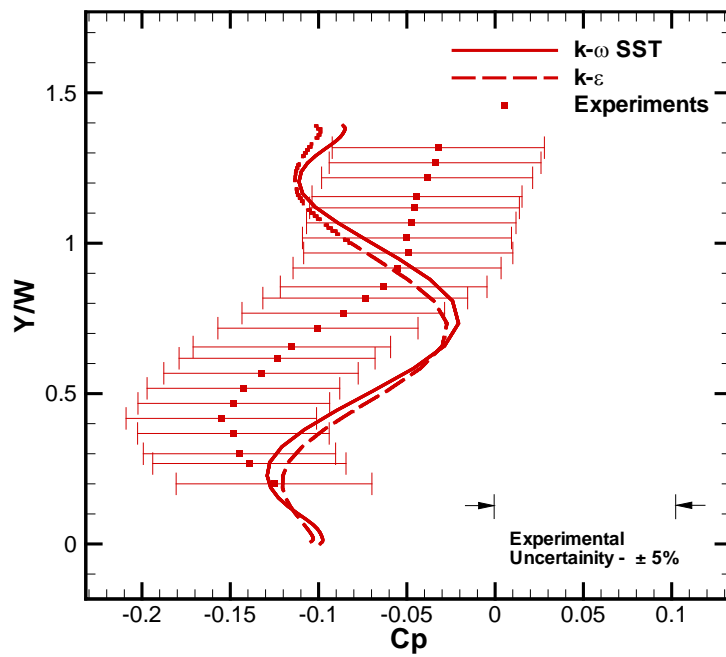


Figure 13: Comparison of the C_p variation on the back of the truck geometry

Subrahmanya Veluri
 Joint Computational/Experimental Aerodynamic Study of a Simplified Tractor/Trailer Geometry

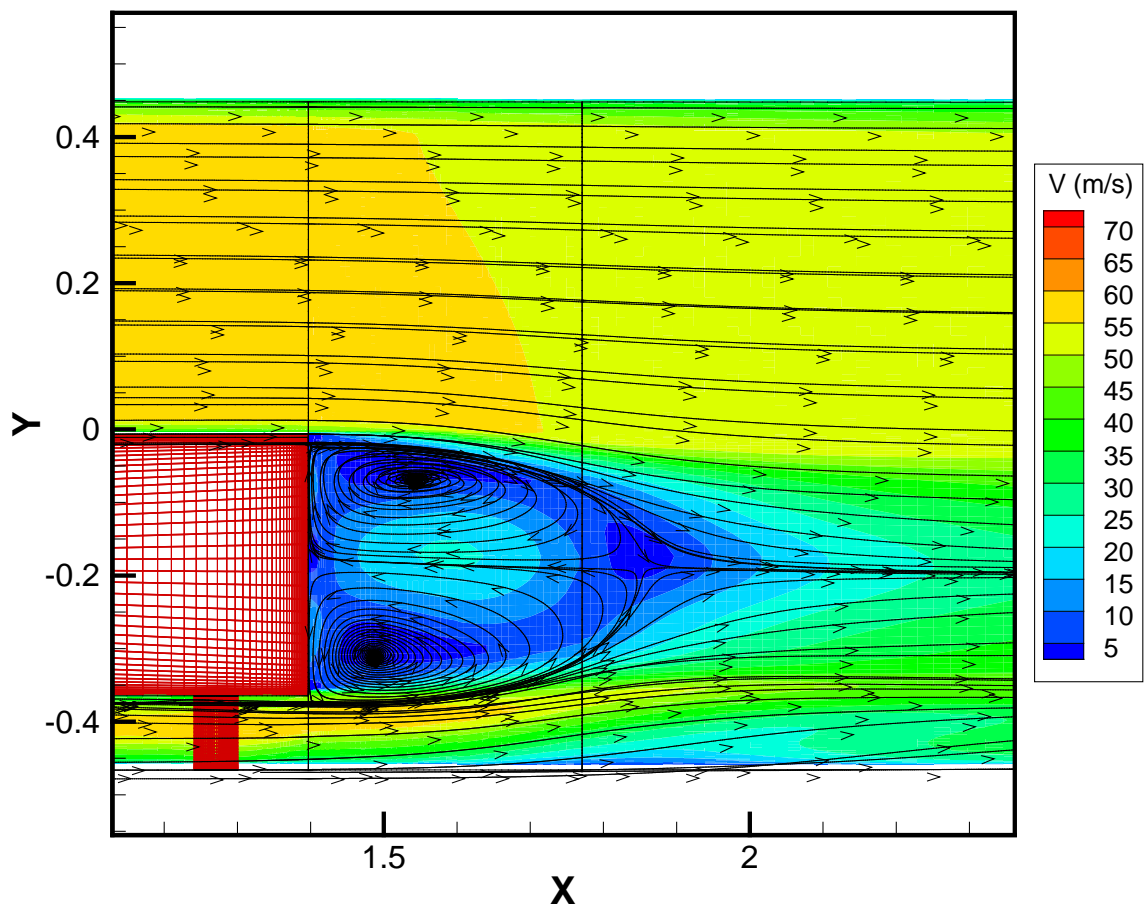


Figure 14: The velocity contours along with the streamlines on the vertical symmetry plane for the SST $k-\omega$ turbulence model

Subrahmanya Veluri
 Joint Computational/Experimental Aerodynamic Study of a Simplified Tractor/Trailer Geometry

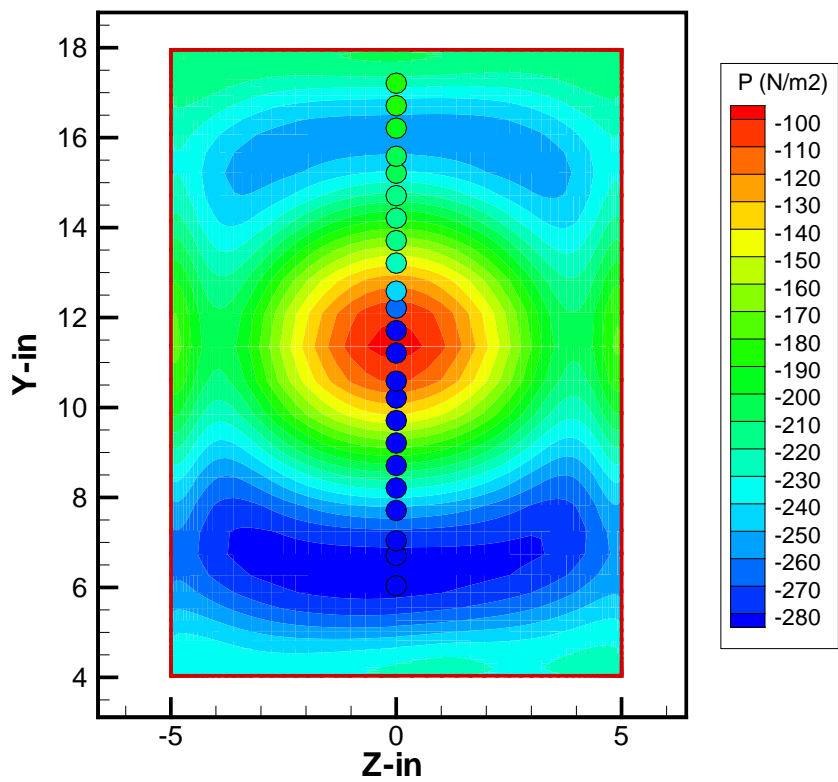


Figure 15: Pressure data comparisons on the back of the trailer

Subrahmanya Veluri

Joint Computational/Experimental Aerodynamic Study of a Simplified Tractor/Trailer Geometry

List of Figures:

Figure 1: Flow visualization/force model mounted in the wind tunnel test section..... 17
Figure 2: Schematic of the simplified truck geometry in the wind tunnel..... 18
Figure 3: Computational geometry of the simplified tractor/trailer placed in the wind tunnel..... 19
Figure 4: Top view of the wind tunnel geometry 20
Figure 5: Comparison of boundary layer profiles (a) at 9 in (b) at 20 in (c) at 39 in from the beginning of the test section..... 21
Figure 6: Flow angularity at vertical center at 9 inches from the beginning of the test section..... 22
Figure 7: Computational mesh (coarse grid) for the truck geometry placed in the wind tunnel..... 23
Figure 8: Drag convergence on truck 24
Figure 9: Schematic of the location of the pressure ports on the truck geometry..... 25
Figure 10: Comparison of the Cp variation on the top and bottom of the truck geometry 26
Figure 11: Comparison of the Cp variation on the sides of the truck geometry 27
Figure 12: Comparison of the Cp variation on front of the truck geometry 28
Figure 13: Comparison of the Cp variation on the back of the truck geometry..... 29
Figure 14: The velocity contours along with the streamlines on the vertical symmetry plane for the SST k- ω turbulence model 30
Figure 15: Pressure data comparisons on the back of the trailer..... 31

List of Tables:

Table 1. List of CFD simulations performed 5
Table 2. Comparison of numerical results of boundary layer properties with experimental results..... 9
Table 3. Computational prediction of the overall drag coefficient using different turbulence models..... 12
Table 4. Drag coefficient comparison..... 14